Electronic Supplementary Material (ESI) for Journal of Materials Chemistry A.

Supporting Information

Expediting Polysulfides Catalytic Conversion for Lithium-Sulfur Battery via In-situ Implanted Ultrafine Fe_3O_4 Nanocrystals in Carbon Nanospheres

Zhe Su,[a‡] Mingqi Chen,[a‡] Yankai Pan,[a] Yajiing Liu,[a] Hai Xu,[a] Yayun Zhang*[a] and Donghui Long*[ab]

[a] State Key Laboratory of Chemical Engineering, East China University of Science and Technology, Shanghai 200237, China.

[b] Key Laboratory of Specially Functional Polymeric Materials and Related Technology, East China University of Science and Technology, Shanghai 200237, China.

‡These authors contributed equally to this work.

∗ Corresponding author:

Tel: +86 21 64252924. Fax: +86 21 64252914.

E-mail: longdh@mail.ecust.edu.cn. (Donghui Long); yy.zhang@ecust.edu.cn.(Yayun Zhang)

Fig. S1 SEM image of ferrous gluconate precursor.

Fig. S2 TEM image of porous carbon nanospheres (PCNSs).

Fig. S3 High-resolution C 1s XPS spectrum curves of Fe_3O_4/CNSs.

Fig. S4 Density functional theory (DFT) calculations of adsorption energies of S_8 and S-containing clusters (Li_2S_x, x=8, 6, 4, 2, 1) on Fe_3O_4(400) (a-f) and amorphous carbon (g-i), respectively.

Fig. S5 Illustration of the electrode reactions for the redox peaks.

Fig. S6 CV curves of Li_2S_6 symmetrical cells with (a) Fe_3O_4/CNSs and (b) PCNSs sulfur-free electrodes at different scan rate.

Fig. S7 SEM image of commercial Celgard 2500 polypropylene membrane (PP).

Fig. S8 The digital photographs of Fe_3O_4/CNSs functionalized separator (a) pristine polypropylene membrane side, (b) after folding.

Fig. S9 Digital photo of electrolyte wettability experimental for the (a) Fe_3O_4/CNSs-PP separator and (b) blank PP separator.

Fig. S10 Thermogravimetric analysis (TGA) curve and derivative thermogravimetric (DTG) curve of pure sulfur cathode under N_2 atmosphere.

Fig. S11 Electrochemical impedance spectroscopy (EIS) plots for the Fe_3O_4/CNSs-PP cell, PCNSs-PP cell and blank PP cell before cycles.

Fig. S12 Galvanostatic charge/discharge voltage profiles for Fe_3O_4/CNSs-PP cell, PCNSs-PP cell and blank PP cell at a current density of 0.2 C.

Fig. S13 Galvanostatic charge/discharge voltage profiles for (a) Fe_3O_4/CNSs-PP cell, (b) PCNSs-PP cell and (c) blank PP cell at different current density.

Fig. S14 CV curves of (a) Fe_3O_4/CNSs-PP cell, (b) PCNSs-PP cell and (c) blank PP cell at different scan

rate. (d-f) Diffusion coefficient linear fitting plots of lithium ion at peak A~C, respectively.

Table S1 Detailed pore parameters of Fe_3O_4/CNSs and PCNSs.

Table S2 Detailed average rate capacities of Fe_3O_4/CNSs-PP cell, PCNSs-PP cell and blank PP cell.

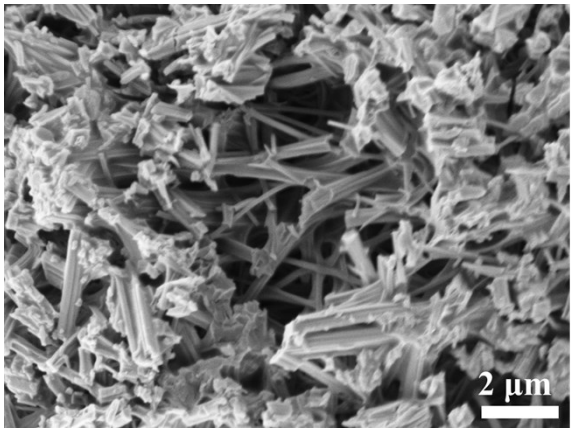

Fig. S1 SEM image of ferrous gluconate precursor.

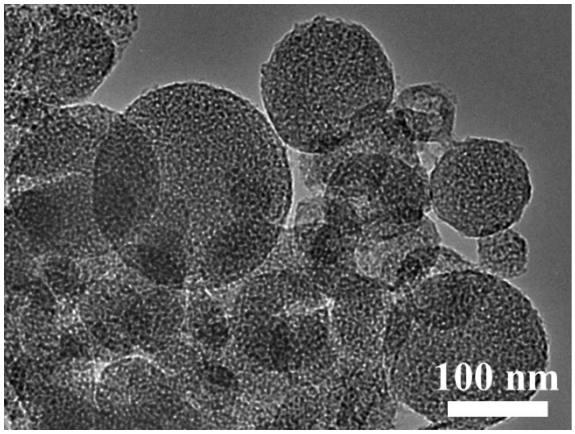

Fig. S2 TEM image of porous carbon nanospheres (PCNSs).

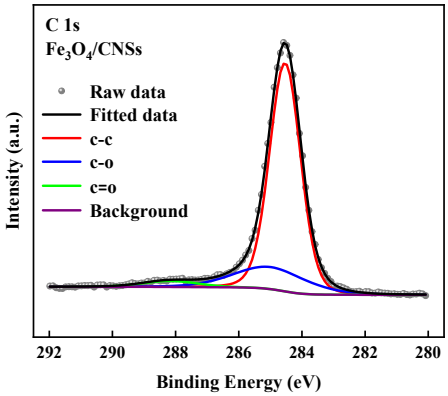

Fig. S3 High-resolution C 1s XPS spectrum curves of Fe_3O_4/CNSs

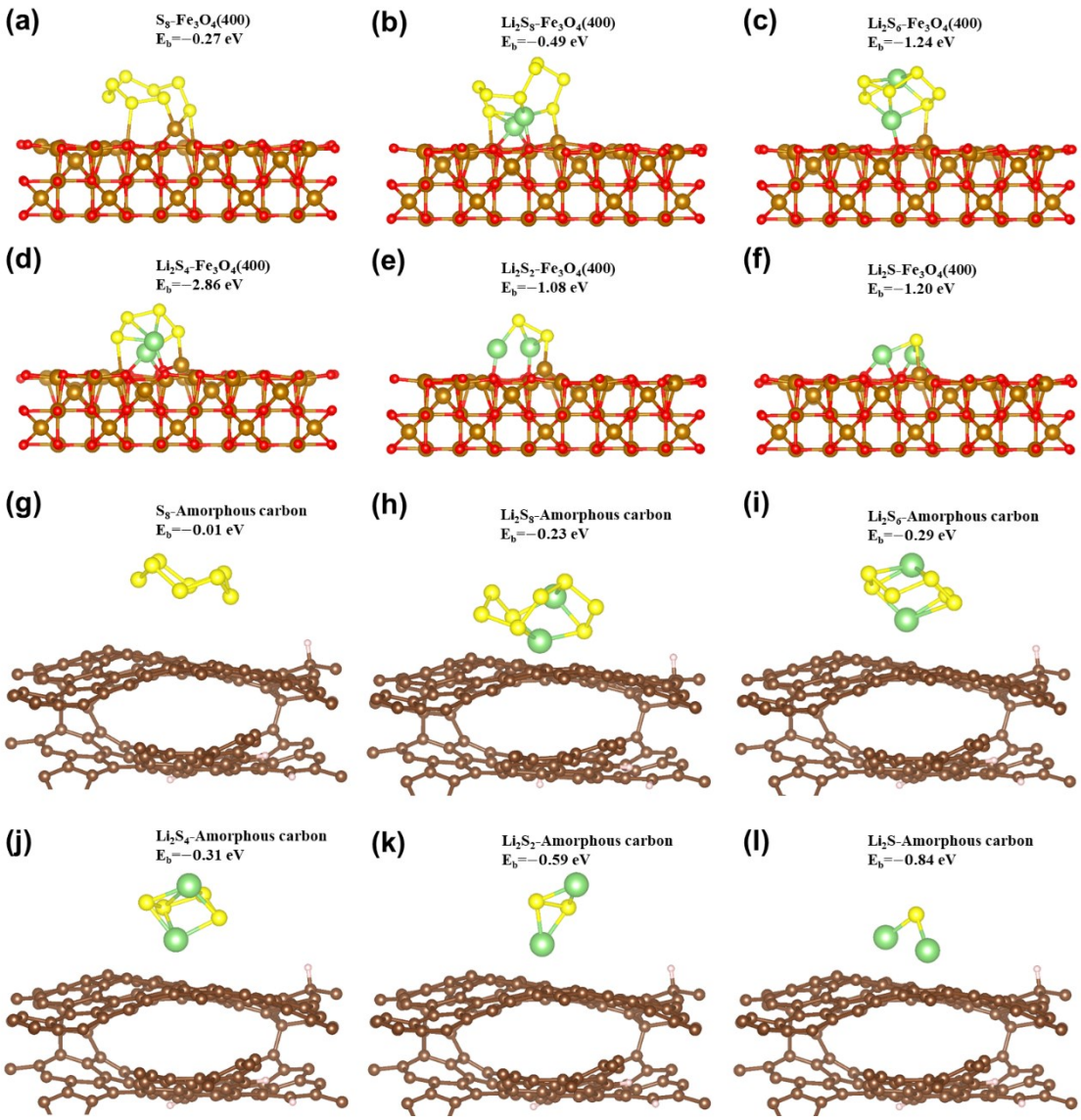

Fig. S4 Density functional theory (DFT) calculations of adsorption energies of S_8 and S-containing clusters (Li_2S_x, x=8, 6, 4, 2, 1) on Fe_3O_4(400) (a-f) and amorphous carbon (g-i), respectively.

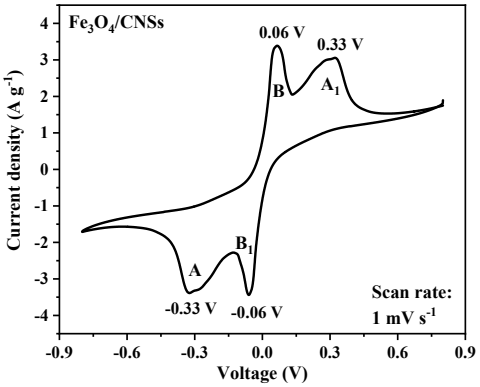

Fig. S5 Illustration of the electrode reactions for the redox peaks.

Since Li_2S_6 was the initial redox active species in the electrolyte, it is reasonable to assume that the Li_2S_6 conversion process on the working electrode can be described as four step reactions as follows: Li_2S_6 was reduced to Li_2S (or Li_2S_2) on the working electrode and oxidized to sulfur on the counter electrode in the cathodic scan peak A (-0.33 V). In the following anodic scan, the rebuilding of Li_2S_6 by the oxidation of Li_2S (or Li_2S_2) on the working electrode and the reduction of sulfur on the counter electrode, which constituted the peak B (0.06 V). Li_2S_6 was oxidized to sulfur on the working electrode and reduced to Li_2S (or Li_2S_2) on the counter electrode in Peak A_1 (0.33 V). Last, in peak B_1 (-0.06 V), Li_2S_6 is formed by the reduction of sulfur on the working electrode and the oxidation of Li_2S (or Li_2S_2) on the counter electrode.[1-3]

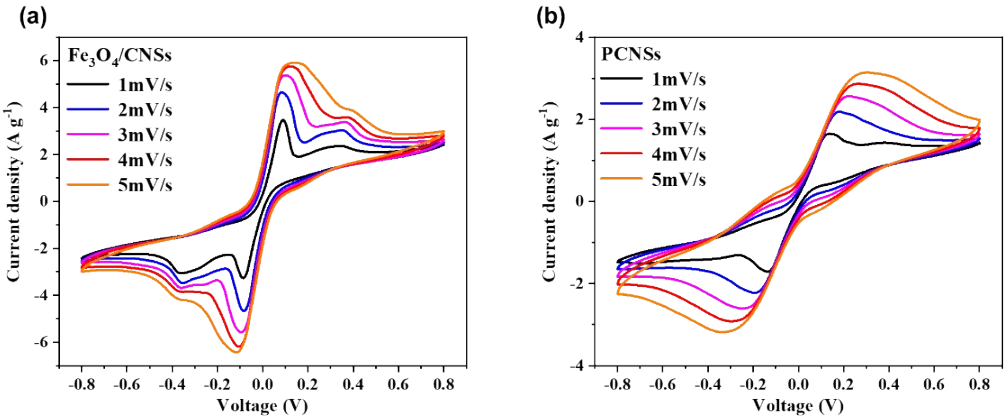

Fig. S6 CV curves of Li_2S_6 symmetrical cells with (a) Fe_3O_4/CNSs and (b) PCNSs sulfur-free electrodes at different scan rate.

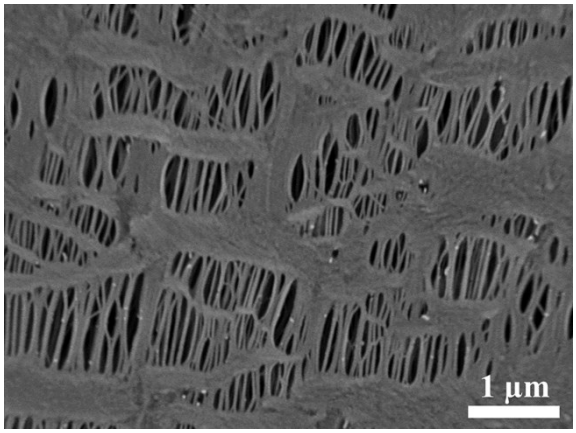

Fig. S7 SEM image of commercial Celgard 2500 polypropylene membrane (PP).

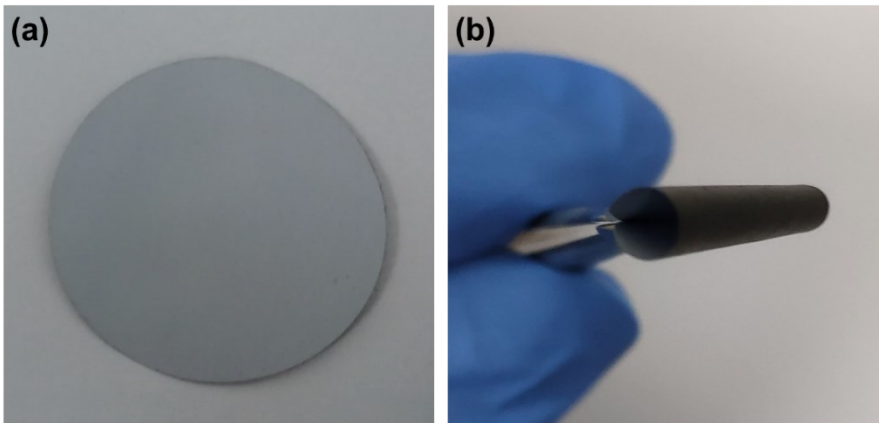

Fig. S8 The digital photographs of Fe_3O_4/CNSs functionalized separator (a) pristine polypropylene membrane side, (b) after folding.

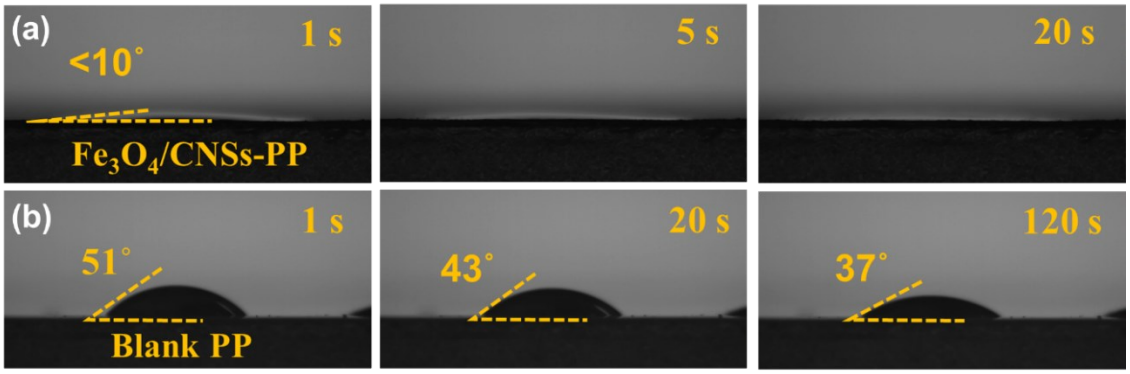

Fig. S9 Digital photo of electrolyte wettability experimental for the (a) Fe_3O_4/CNSs-PP separator and (b) blank PP separator.

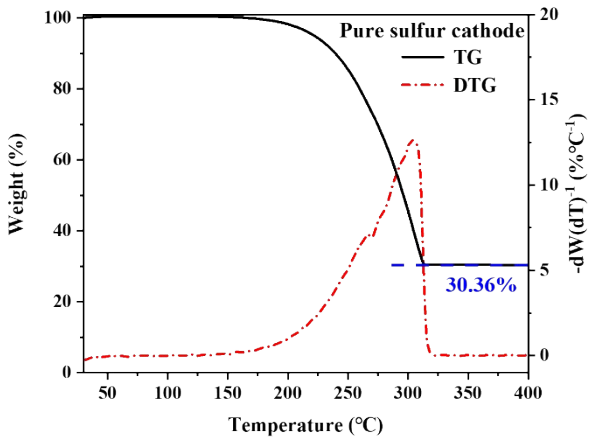

Fig. S10 Thermogravimetric analysis (TGA) curve and derivative thermogravimetric (DTG) curve of pure sulfur cathode under N_2 atmosphere.

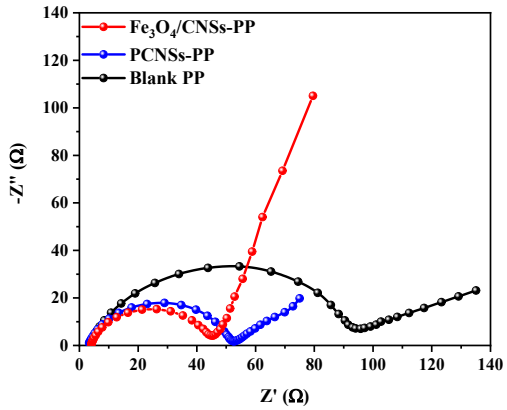

Fig. S11 Electrochemical impedance spectroscopy (EIS) plots for the Fe_3O_4/CNSs-PP cell, PCNSs-PP cell and blank PP cell before cycles.

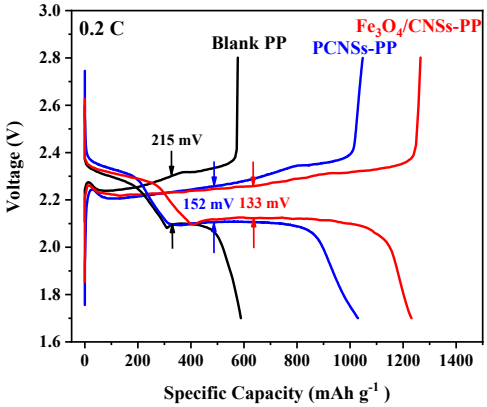

Fig. S12 Galvanostatic charge/discharge voltage profiles for Fe_3O_4/CNSs-PP cell, PCNSs-PP cell and blank PP cell at a current density of 0.2 C.

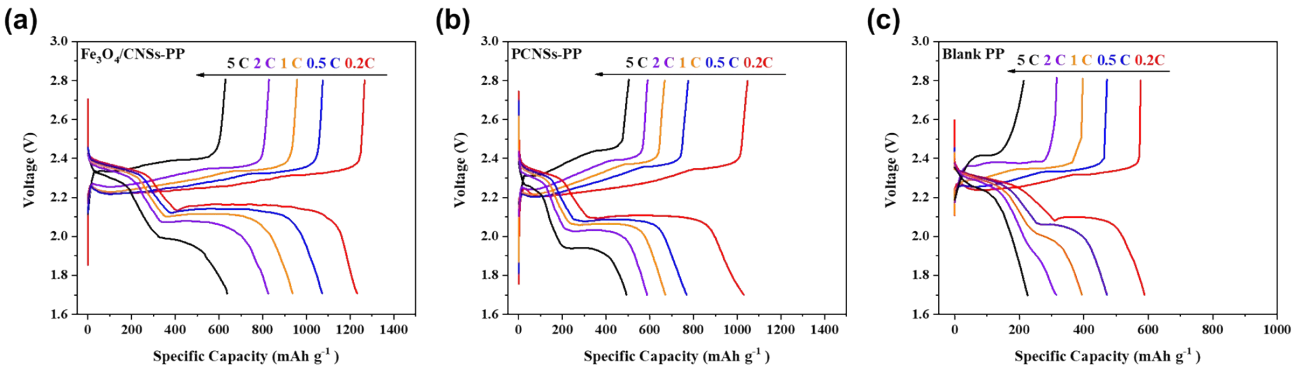

Fig. S13 Galvanostatic charge/discharge voltage profiles for (a) Fe_3O_4/CNSs-PP cell, (b) PCNSs-PP cell and (c) blank PP cell at different current density.

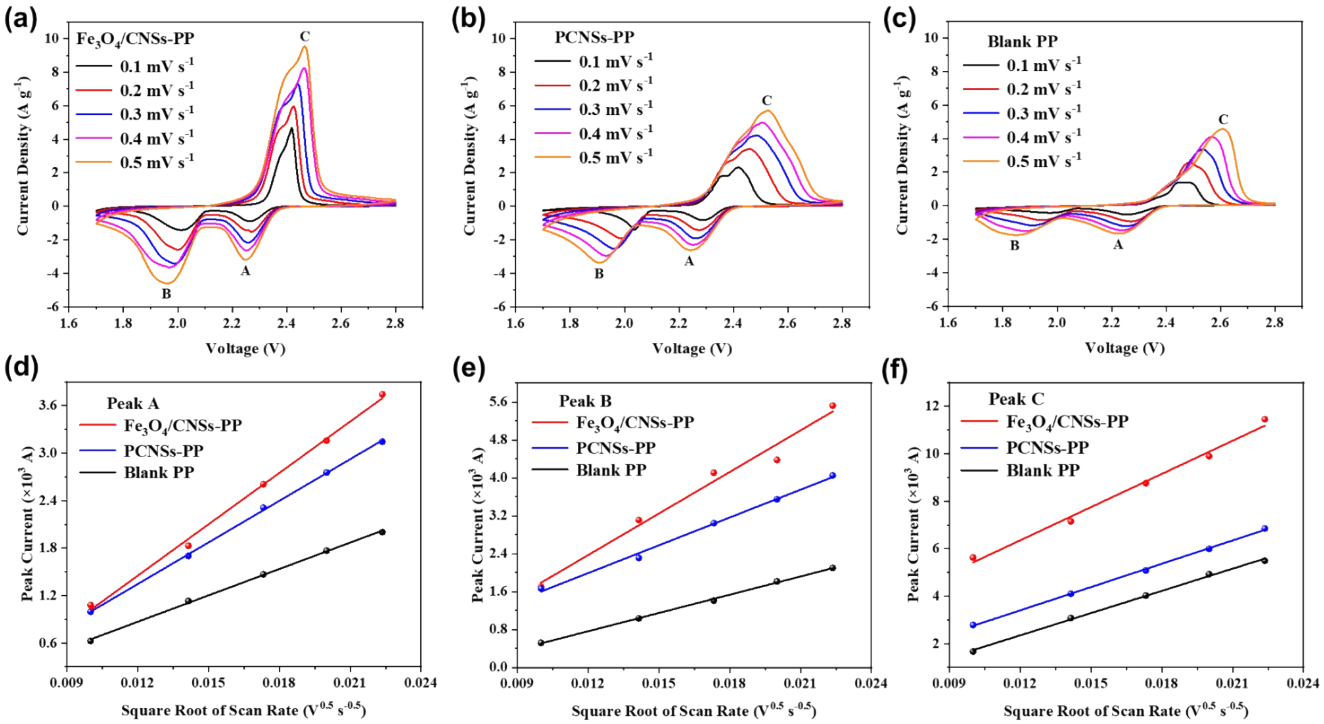

Fig. S14 CV curves of (a) Fe_3O_4/CNSs-PP cell, (b) PCNSs-PP cell and (c) blank PP cell at different scan rate. (d-f) Diffusion coefficient linear fitting plots of lithium ion at peak A-C, respectively.

Table S1 Detailed pore parameters of Fe_3O_4/CNSs and PCNSs.

Sample	S_{BET} ($m^2\ g^{-1}$)	S_{Micro} ($m^2\ g^{-1}$)	V_{Total} ($cm^3\ g^{-1}$)	V_{Micro} ($cm^3\ g^{-1}$)
Fe_3O_4/CNSs	247	73	0.41	0.04
PCNSs	799	317	0.84	0.16

Table S2 Detailed average rate capacities of Fe_3O_4/CNSs-PP cell, PCNSs-PP cell and blank PP cell.

Rate	Fe_3O_4/CNSs-PP	PCNSs-PP	Blank PP
	mAh g^{-1}	mAh g^{-1}	mAh g^{-1}
0.2 C	1225	959	614
0.5 C	1068	755	496
1 C	947	669	431
2 C	828	596	358
5C	649	500	228

References:

1. H. Lin, L. Yang, X. Jiang, G. Li, T. Zhang, Q. Yao, G. W. Zheng and J. Y. Lee, Energy Environ. Sci., 2017, 10, 1476-1486.
2. H. Lin, S. Zhang, T. Zhang, H. Ye, Q. Yao, G. W. Zheng and J. Y. Lee, Adv. Energy Mater., 2018, 8.
3. P. Guo, K. Sun, X. Shang, D. Liu, Y. Wang, Q. Liu, Y. Fu and D. He, Small, 2019, 15, 1902363.